

# Magnetically-activated accretion outbursts of pre-main sequence discs

Jacob Cleaver<sup>1</sup>, Lee Hartmann<sup>1</sup>, Jaehan Bae<sup>2</sup> 

<sup>1</sup>*Department of Astronomy, University of Michigan, 1085 S. University Ave, Ann Arbor, MI 48105, USA*

<sup>2</sup>*Department of Astronomy, University of Florida, 316 Bryant Space Science Building, Gainesville, FL 32611, USA*

Accepted XXX. Received YYY; in original form ZZZ

## ABSTRACT

We investigate whether triggering of the magnetorotational instability (MRI) in protoplanetary discs can account for the wide diversity of observed accretion outbursts. We show that short-lived, relatively low accretion rate events probably result from triggering in the inner disc and can occur at low surface densities, comparable to or smaller than the minimum mass solar nebula, and thus are very unlikely to result from MRI triggering by gravitational instability. We develop time-dependent accretion disc models using an  $\alpha$ -viscosity approach and calculate light curves to compare with observations. Our modeling indicates that the lag time between infrared and optical bursts seen in Gaia 17bpi can be explained with an outside-in propagation with an  $\alpha \sim 0.1$  in the MRI-active region, consistent with other estimates. While outbursts in inner discs can show time delays of a few years between infrared and optical light curves, our models indicate that large, FU Ori-like bursts can exhibit infrared precursors decades before optical bursts. Detecting such precursors could enable analysis of the central star before it is overwhelmed by the rapid accreting material, as well as constraining outburst physics. Our results emphasize the importance of near-infrared monitoring of young stellar objects in addition to optical surveys. In addition, our findings emphasize the need for more sophisticated, three-dimensional, non-ideal magnetohydrodynamic simulations to fully exploit observational results.

**Key words:** accretion, accretion discs – protoplanetary discs – stars:pre-main sequence

## 1 INTRODUCTION

Potential or actual planet-forming discs accrete at variable rates onto their young central stars (see references in [Hartmann et al. 2016](#)). In some cases accretion rates can change by orders of magnitude over timescales of months to years. Such accretion events or outbursts can provide insights into mechanisms of mass transport that are otherwise difficult to constrain. Outbursts also can result in significant thermal processing of protoplanetary material ([Bell et al. 2000](#); [Ciesla 2007, 2010](#)). The amount of material transported in accretion bursts also indicates lower limits to mass reservoirs of inner discs.

The largest accretion outbursts are those of the FU Orionis variables ([Herbig 1977](#); [Hartmann & Kenyon 1996](#)), that can involve accretion at rates  $\sim 10^{-5} - 10^{-4} M_{\odot} \text{ yr}^{-1}$  lasting tens of years up to 100 years or more. While such outbursts are relatively rare, the advent of systematic wide-field photometric surveys have turned up increasing numbers of FUors (see [Audard et al. 2014](#); [Fischer et al. 2022](#), for reviews). Several different mechanisms have been proposed to explain FUor outbursts; accretion from a disc that causes the central star to expand ([Larson 1983](#)), fragments resulting from gravitational instability (GI) ([Vorobyov & Basu 2006, 2010](#)), disruption of young massive planets ([Nayakshin & Lodato 2012](#); [Nayakshin et al. 2023](#)), encounters with companion stars ([Forgan & Rice 2010](#)), planet-disc interaction ([Lodato & Clarke 2004](#)), and GI-driven turbulence that triggers the magnetorotational instability (MRI; [Armitage et al. 2001](#);

[Zhu et al. 2007, 2009, 2010a,b](#); [Bae et al. 2013, 2014](#); [Kadam et al. 2020](#)) (see [Vorobyov et al. 2021](#), for a discussion).

Mass and angular momentum transport in pre-main sequence discs is generally thought to be slow. The low ionization states thought to be characteristic of these discs is believed to preclude efficient transport by the MRI. Observations also indicate that levels of turbulence, whether hydrodynamic or magnetic, are very low (at least in outer discs; ([Flaherty et al. 2015, 2020](#)), consistent with slow transport rates. Models of magnetic wind-driven accretion ([Bai & Stone 2013b,a](#); [Bai et al. 2016](#)) do predict rapid global accretion flows, but these are confined to thin upper layers of the disc, only draining the bulk of the mass over long timescales. However, if for some reason the disc temperatures can rise above  $\sim 1000 - 1200$  K, the rapid increase in thermal ionization can result in activating the MRI ([Desch & Turner 2015](#)), with a corresponding large increase in angular momentum transport that results in an accretion outburst. In support of this picture, the FU Ori objects show optical and near-infrared spectra of gaseous photospheres with local effective temperatures  $\gtrsim 2000$  K, easily large enough to produce sufficient thermal ionization for the MRI to operate.

Photometric surveys are increasingly finding outbursting objects with smaller accretion rates than in the canonical FU Ori objects (e.g., [Contreras Peña et al. 2014](#); [Lucas et al. 2017](#); [Park et al. 2021](#); [Hillenbrand et al. 2018](#); [Contreras Peña et al. 2023](#)). Such events may be difficult to explain with triggering by gravitational turbulence, as GI requires high surface densities that tend to produce high accretion rates. Nevertheless, the spectral signatures of many of

\* E-mail: lhartm@umich.edu

these smaller bursts (e.g., optical effective temperatures) are similar to those of FUors, indicating that activation of the MRI is likely.

Recent observations of two outbursting events, Gaia 17bpi (Hillenbrand et al. 2018; Rodriguez & Hillenbrand 2022), and Gaia 18dvy (Szegeedi-Elek et al. 2020), are of particular interest in that the outbursts clearly start earlier at near-infrared wavelengths than in the optical regime. This behavior shows that the outbursts are propagating outside-in, with the increase in temperature appearing first at large radii where the discs are cooler. In principle, the time lapse between the optical and infrared light curves yield constraints on the propagation speed of the outburst and other physical parameters.

These recent observational developments motivate this effort to compute outburst light curves using time-dependent simulations in a preliminary exploration of what might be learned from present and future observations.

## 2 OVERVIEW OF CONDITIONS FOR MRI ACTIVATION

To set the stage for understanding the behavior of the numerical simulations, and the resultant outburst light curves, we outline some basic considerations. Activation of the MRI by thermal ionization in the outer disc requires temperatures well in excess of those attainable either by irradiation heating from the central star or internal viscous heating at typical T Tauri accretion rates. For a steady disc the effective temperature resulting from viscous heating well beyond the inner radius is

$$T_e \sim 60 M_{0.3}^{1/4} \dot{M}_{-8}^{1/4} R_{au}^{-3/4}, \quad (1)$$

where  $M_{0.3}$ ,  $\dot{M}_{-8}$ , and  $R_{au}$  are the stellar mass in units of  $0.3 M_\odot$ , the accretion rate in units of  $10^{-8} M_\odot \text{ yr}^{-1}$ , and the radius in au. Even during a massive outburst with  $\dot{M} = 10^{-4} M_\odot \text{ yr}^{-1}$ , the effective temperature at 1 au would only be  $\sim 600$  K. Thus activating and maintaining the MRI requires the central temperature to be larger than that of the surface, especially from the quiescent state at typical T Tauri accretion rates of  $\sim 10^{-8} M_\odot \text{ yr}^{-1}$ . Models that can achieve this require radiative trapping, which in turn requires the disc to be significantly optically-thick (Armitage et al. 2001; Zhu et al. 2009, 2010a,b).

To fix ideas, consider a simple model along the lines of Zhu et al. (2010a,b). We suppose that some mechanism produces a local jump in the temperature, high enough to make a transition from the low-viscosity initial state to an MRI-active state. The resulting viscous heating is (e.g., Bell & Lin 1994)

$$F_V = \frac{9}{4} \alpha \Omega c_s^2 \Sigma. \quad (2)$$

Here we employ the ‘‘alpha’’ viscosity formalism, where  $\Omega$  is the Keplerian angular frequency,  $c_s$  is the (midplane) sound speed, and  $\Sigma$  is the surface density. We also assume that this increase in energy generation is instantaneously balanced by radiative losses of the optically-thick disc with effective temperature  $T_e$ ,

$$F_V = 2\sigma T_e^4, \quad (3)$$

with a factor of two to account for both sides of the disc. Radiative trapping raises the central temperature  $T_c$  at large optical depth relative to the effective temperature  $T_e$  such that (Hubeny 1990; Zhu et al. 2010a)

$$T_e^4 = \frac{8}{3} \frac{T_c^4}{\tau_R}, \quad (4)$$

where  $\tau_R = \kappa_R \Sigma$  is the Rosseland mean optical depth. (Here we ignore heating by irradiation from the central star for simplicity.)

While the Rosseland mean opacity  $\kappa_R$  generally depends upon temperature and density, here we only establish a critical surface density at a particular activation temperature. Following the results of (Desch & Turner 2015) that indicate activation temperatures lower than those that would result in sublimation of grains, we assume that the opacity is dominated by dust. This allows us to simplify the solution by adopting a constant value for  $\kappa_R$ , since the temperature and density dependences are weak (Zhu et al. 2009). As shown later in discussing FU Ori-type large bursts, our results are broadly consistent with the following numerical simulations and with our previous calculations that explicitly use the temperature and density dependence of the opacity (Zhu et al. 2010a,b; Bae et al. 2013).

Substituting for  $T_e$  on the right-hand side of equation 3 using equation 4, setting  $T_c = T_i$ , the adopted activation temperature, and solving for the surface density results in

$$\Sigma_i^2 = \frac{64\sigma}{27} \frac{\mu}{\alpha\Omega\mathcal{R}} \frac{T_i^3}{\kappa_R}, \quad (5)$$

where  $\mu$  is the mean molecular weight and  $\mathcal{R}$  is the gas constant. This is the limiting surface density needed to raise the central temperature to  $T_i$ , given  $\alpha$ ,  $\Omega$ , and  $\kappa_R$ . For fixed values of  $\alpha$  and  $\kappa$ ,  $\Sigma_i \propto R^{3/4}$ . Thus, it is easier to trigger the MRI at smaller radii, as temperatures are naturally higher.

Thus, equation 5 indicates that there will be a minimum value of the surface density at which the MRI can be sustained, with  $\Sigma_c \propto T_i^{3/2} \alpha^{-1/2} \kappa^{-1/2} R^{3/2}$  for a given central star mass  $M$ . The numerical simulations presented in the following sections exhibit this basic scaling, although with significantly larger values. This is because this steady-state model does not account for time-dependent changes in  $\Sigma$ , as discussed in the following section.

## 3 TIME-DEPENDENT OUTBURST MODELS

### 3.1 Methods

A full treatment of triggering the MRI in a protoplanetary disc would require three-dimensional, non-ideal magnetohydrodynamic (MHD) calculations in a resistive disc with radiative transfer. To our knowledge such calculations have not yet been conducted and would in any case be subject to considerable uncertainties (for example, the properties and spatial distribution of dust). Given these complexities, a simpler approach is warranted to outline basic issues.

We computed time-dependent 1-dimensional disc models using the equations and methods described in Zhu et al. (2010a), with a few small modifications. The disc has an MRI-active layer with surface density  $\Sigma = 10 \text{ g cm}^{-2}$ , or is otherwise non-viscous, with a central ‘‘dead zone’’ unless the temperature is raised above some fiducial value. In this case we turn on the viscosity  $\alpha$  parameter to its full value smoothly as the temperature rises from 1200 K to 1300 K, on an e-folding timescale of  $2\Omega^{-1}$ , where  $\Omega$  is the Keplerian angular frequency (see equation 17 in Zhu et al. (2010a)), but without the second term for radial diffusion of the magnetic field; we find that that term makes essentially no difference. As discussed in the Appendix, modest changes in the activation temperature do not significantly change results. The active layer plays essentially no role in these calculations other than setting a base low accretion rate  $\dot{M} \lesssim 10^{-9} M_\odot \text{ yr}^{-1}$ , which does not have a significant impact on the outburst light curves. Most models were calculated with 256 grid steps over ranges from  $\sim 0.1$  to 10 au, with a few test models run with 512 radial steps.

We assume that when the MRI is activated it results in a maximum

viscosity parameter  $\alpha = 10^{-1}$ . This choice is motivated by results for Gaia 17bpi that are strongly inconsistent with observations assuming  $\alpha = 0.3$  and  $\alpha = 0.03$  (see Appendix).

We adopt the opacities given by [Zhu et al. \(2009\)](#), except we reduce the opacities below 1400 K by a factor of ten to simulate depletion of small grains. Unlike previous papers ([Zhu et al. 2010a,b](#); [Bae et al. 2013, 2014](#)) there is no infall to the disc. In addition, we weaken the transport due to gravitational instability by setting the viscosity due to GI as  $\alpha_Q = 0.05 \exp(-Q^4)$ , where  $Q = c_s \Omega / (\pi G \Sigma)$  is the Toomre parameter. This was done to focus on the conditions needed for MRI-triggering in more generality than using GI heating.

We impose a high central temperature perturbation at a given radius, as we are agnostic about the source of this energy release. A top-hat temperature increase to  $T = 1500\text{K}$  in a specified radial range is assumed. Whether or not an outburst occurs depends mostly on the magnitude of the surface density  $\Sigma$  at the position of the temperature increase and to some extent on the radial width of the perturbation. These details depend upon our assumption of a constant  $\alpha$  among other things; as we are most interested in the light curves assuming the MRI is triggered, these details are unlikely to change the main results.

Our initial surface density distributions are for the most part assumed to be flat inside the radius of the temperature perturbation, with a decline at longer radii. The choice of an inner flat  $\Sigma(R)$  is motivated by several reasons, beyond simplicity: (1) Our results in [Hartmann & Bae \(2018\)](#) for viscous disc accretion at low values of  $\alpha$  lead to fairly flat density distributions (as illustrated in §3.3). (2) Our simulations for FU Ori objects show that the inner disc becomes depleted after the first outburst ([Zhu et al. 2010b](#); [Bae et al. 2013](#)). The detailed  $\Sigma(R)$  is not completely flat, but experiments indicate that outburst properties are not sensitive to modest (factor of 2-3) variations. (3) Simulations with steeply increasing  $\Sigma(R)$  are prone to generate inside-out bursts, in contrast to most observations (see following discussion). (4) The choice of a flat density distribution does not affect the outburst, but minimizes the peak accretion rate, as discs with more mass at smaller radii accrete more. On the other hand, a decreasing surface density with radius in the outer disc is adopted to avoid GI-triggering, which we have already explored for FU Ori outbursts ([Zhu et al. 2010b](#); [Bae et al. 2013](#)).

To calculate the optical spectrum it is necessary to capture regions where the disc is hottest. This means we must adopt small innermost radii = 0.01 – 0.015 au, much smaller than typically used in our previous calculations ([Zhu et al. 2010b](#); [Bae et al. 2013, 2014](#)) and in other simulations ([Vorobyov & Basu 2006, 2010](#); [Vorobyov et al. 2020](#); [Kadam et al. 2020](#)).<sup>1</sup> If there is a significant surface density at such radii, the heating of the disc by irradiation from the central star will make the innermost radii MRI-active (e.g. [Gehrig et al. 2022](#)). This can result in oscillating behavior at the transition between active and inactive regions (see, for instance, the rapid oscillations in accretion rate seen at early times in Figures 2 and 3 in [Bae et al. 2013](#)).

More generally, the activation of the MRI at the inner disc edge produces an inside-out burst. This is not a difficulty for models for which the main temperature perturbation is taken to be at large radii, because the initial inside-out event can die out first. However, models comparable to the observations of Gaia 17bpi need to be perturbed at small radii to produce the necessary short timescales, and it is easy for the

inside-out burst, that would exhibit little to no lag between infrared and optical light curves, to wipe out the outside-in outburst. The structure of the inner region is further complicated by the likely presence of the stellar magnetosphere, which typically truncates the disc at 3-5 stellar radii ([Bouvier et al. 2020](#); [Gravity Collaboration et al. 2020](#)). With stellar radii  $\sim 1 - 2R_\odot$ , this implies disc truncation at about 0.015 – 0.025 au ( $\sim 3 - 5R_\odot$ ). As our interest is in outbursts, we avoid constructing a self-consistent steady inner disc structure, by adopting a low irradiation temperature  $T_{ext} = 1200(r/0.15\text{au})^{-1/2}$  and adopt a low surface density inside of  $\sim 0.02$  au, depending on the model. This means that the pre-outburst accretion rates are not reliable, but as we are interested in the behavior of outbursts the very innermost disc pre-burst state makes little difference to the burst light curves.

### 3.2 Basic behavior

In analyzing the model results we did not conduct a broad search of parameter space, because the accuracy with which our simple  $\alpha$  viscosity models can represent non-ideal MHD results is uncertain. Instead, we focus on broad trends that hopefully can ultimately be tested by observations.

The basic behavior of our outburst models are broadly similar to those presented in earlier papers ([Zhu et al. 2010a,b](#); [Bae et al. 2013, 2014](#)). Figures 1 and 2 show snapshots of the disc temperature and surface density distributions at selected times assuming a temperature perturbation at 1 au at  $t = 0$ . During the initial propagation of the outburst (second panels,  $t = 125$  yr), the large increase in  $\alpha$  in the central regions from very low initial values causes mass to both move inward in a dense front, while moving outward at larger radii to conserve angular momentum. This results in a surface density minimum near the site of the original perturbation.

The accretion wave tends to move inward at a temperature  $\sim 1500$  K; this is a thermostatic effect of the assumed evaporation of dust (see, e.g. [D’Alessio et al. 2001](#)), assuming the [Zhu et al. \(2009\)](#) opacity. However, once the wave moves inward of about 0.5 au, the temperature makes a dramatic jump to very high values. This is due to the thermal instability that occurs once the dust is gone, because of the steep temperature dependence of the gas opacity ([Bell & Lin 1994](#)). Note that though the central temperature exhibits jumps, the surface (effective) temperature closely follows the  $T \propto R^{-3/4}$  distribution characteristic of the optically-thick steady disc.

The accretion front does not reach the inner edge of the disc until  $t \sim 175$  yr (Figure 3). The high surface density and high viscosity of the hot inner region results in a large, fast jump in the accretion rate. There are also brief “drop-outs” in  $\dot{M}$  as the outburst proceeds. The reason for the accretion dips is understandable from an inspection of the final panels in Figures 1 and 2 at  $t = 183$  yr. The inner disc surface density at this time has decreased by an order of magnitude from the preceding snapshot at  $t = 175$  yr. Because the temperature of the inner disc is much higher than that of the outer disc, and the viscosity is assumed to scale as  $\nu \propto \alpha T$ , the mass transport is much faster in the inner hot region than in the outer, cooler zone. This results in the depletion of mass in the hot inner region of mass until transport from the cooler region can replenish the material. In essence, this is a version of the “S-curve” thermal instability mechanism for repeated outbursts (see [Bell & Lin 1994](#), and references therein).

Rapid, temporary dips in brightness have been observed in the FU Ori objects V1057 Cyg and V1515 Cyg ([Kolotilov & Kenyon 1997](#); [Kenyon et al. 1991](#); [Kopatskaya et al. 2013](#); [Szabó et al. 2022](#)), with perhaps a longer, somewhat different drop seen in V2493 Cyg ([Semkov et al. 2021](#)). Whether these observed dips are the result of

<sup>1</sup> We note that [Gehrig et al. \(2022\)](#) did consider small inner radii but concentrated on the interaction with the stellar magnetosphere and consequent evolution of stellar rotation, not the resulting spectra.

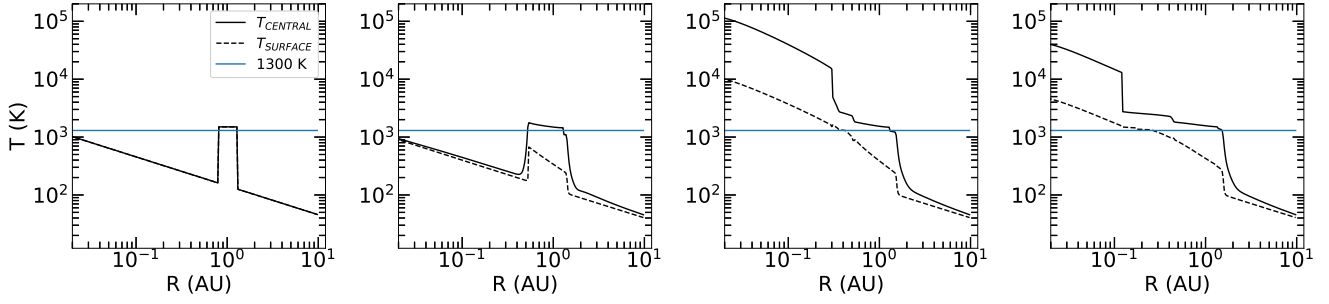


**Figure 1.** The central temperature (solid line) and the surface temperature (dashed line) at  $t = 0, 125, 175,$  and  $183$  years (compare with Figures 2 and 3). The horizontal line denotes  $T = 1300$  K. The large increase in temperature seen in the last two panels results from thermal instability (see text).

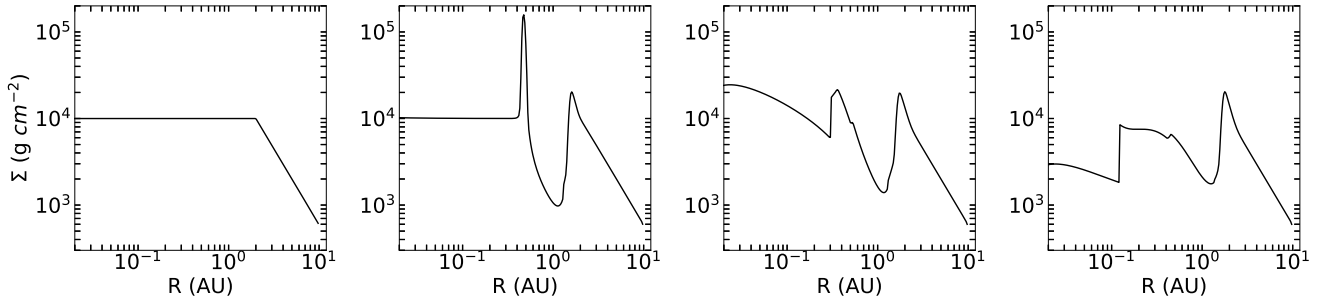


**Figure 2.** Surface densities at the same times as in Figure 1 corresponding to times  $t = 0, 125, 175,$  and  $183$  years (compare with Figure 3). The activation of the MRI, and the resulting jump in viscosity, causes matter to move inward and outward (to conserve angular momentum), resulting in a depletion of mass at the site of the original perturbation.

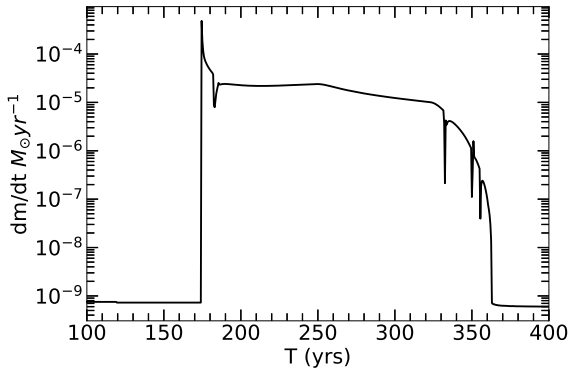


**Figure 3.** Accretion rate at the inner disc edge as a function for the model shown in Figures 1 and 2.

this mechanism, instead of dust extinction events, is not clear. If these are due to an accretion drop-out, one would expect the optical spectrum to have a later spectral type (cooler maximum temperature) during minimum, whereas a dust extinction event would not show a change. Detailed spectral and photometric monitoring would be needed to test this. In any case, it should be emphasized that our 1D models assume axisymmetry, which is unlikely in MHD turbulence, and thus may result in a much bigger effect than in more complex, non-axisymmetric MRI behavior, including convection (Zhu et al. 2010a).

### 3.3 Critical surface density

We constructed a set of outburst models triggered at several different radii. At each position we tried different initial surface densities to find the minimum value of  $\Sigma$  for which the perturbation could be sustained and led to an outburst. The central star mass in all cases was  $0.3M_{\odot}$  and we adopted the irradiation temperature and flat surface density distribution interior to the position of the perturbation as discussed in §3.1, except with an inner ‘‘magnetospheric’’ depletion as needed. The results are shown by the circles in Figure 4.

We can use the developments of §2 to understand the dependence of the critical surface density on radius, but with an important difference. Using equation 5 and adopting the dust opacity from Zhu et al. (2009) reduced by an order of magnitude to account for some depletion of small dust, results in

$$\Sigma_i \sim 1 \times 10^3 (\alpha_{-1} M_{0.3} \kappa_i)^{-1/2} R_{au}^{3/4} T_i^{3/2} \text{ g cm}^{-2}, \quad (6)$$

where  $\kappa_i$  in units of  $0.87 \text{ cm}^2 \text{ g}^{-1}$ ,  $T_i$  is in units of 1300 K, the stellar mass is  $M_{0.3}$  is in units of  $0.3M_{\odot}$ ,  $R_{au}$  is self-evident, and  $\alpha_1$  is in units of 0.1, so that the scaling is appropriate for our simulations.

In Figure 4 we show that while the prediction of equation 6 exhibits the correct dependence on radius, it underpredicts the limiting surface densities in the simulations by a factor of  $\sim 10$ . After considerable exploration it appears that the reason for the discrepancy is the change in  $\Sigma$  due to huge increase in viscosity by the applied temperature perturbation. As shown in the second panel of Figure 2, the activation of the  $\alpha$  viscosity generates a large drop in  $\Sigma$  at the central position of the initial perturbation as mass diffuses away both inward and outward. The magnitude of this decrease in surface density is typically a factor of 10, such that this minimum must be close

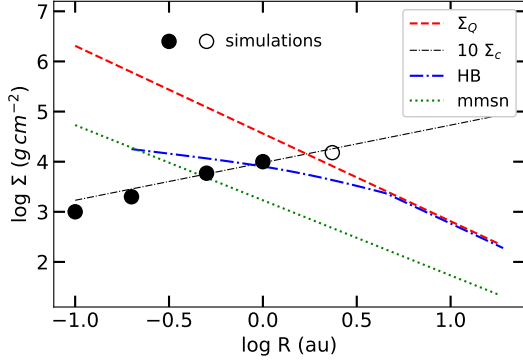


**Figure 4.** Limiting surface densities for outbursts (filled circles) for the standard set of numerical simulations. The open circle denotes a model where the model gravitational viscosity is important. For comparison we show 10 times the “critical” surface density derived in equation 5, along with the limiting value for gravitational instability  $\Sigma_Q$  (dashed line) as an upper bound, the minimum mass solar nebula surface density (dotted line), and a model for low-state accretion at  $2 \times 10^{-8} M_\odot \text{ yr}^{-1}$  and  $\alpha = 3 \times 10^{-4}$  from Hartmann & Bae (2018).

to, or larger than, the value of  $\Sigma_c$  from equation 6 for the outburst to proceed rather than die away. As a specific example, the second panel of Figure 2 shows a minimum value of  $\Sigma \sim 1 \times 10^3 \text{ g cm}^{-2}$ , in agreement with equation 6 at 1 au. Equation 6 indicates how  $\Sigma_c$  would change due to differing adopted parameters other than the radius.

We compare the results in Figure 4 with three different surface density distributions: the limiting value of the surface density for gravitational instability setting  $Q = c_s \Omega / (\pi G \Sigma_Q) = 2$ , assuming  $T_{irr} = 200(R/\text{au})^{-1/2} \text{ K}$  (red dashed line); the canonical minimum-mass solar nebula (green dotted line); and the surface density of a model by Hartmann & Bae (2018) consistent with observed T Tauri accretion rates  $\sim 10^{-8} M_\odot \text{ yr}^{-1}$  for a low state  $\alpha = 3 \times 10^{-4}$ . The comparisons indicate that much lower surface densities can suffice to sustain an MRI-driven outburst at small radii. Conversely, large surface densities are required to trigger the MRI at large radii where the disc is more likely to be gravitationally unstable. Sustaining an MRI outburst at radii greater than a few au would require surface densities far above the limit for gravitational stability, so this predicts an outer limit for the high-temperature region.

### 3.4 Accretion rates and decay timescales

The simulations unsurprisingly predict that larger, longer outbursts result from triggering at larger radii. Figure 5 shows the model sequence for the triggering radii, assuming minimum surface densities, in comparison with observational estimates of mass accretion rates for several objects. Using the new Gaia distance of 416 pc and adopting an inclination of  $i = 35^\circ$ , Zhu et al. (2020) estimated an accretion rate of  $\sim 4 \times 10^{-5} M_\odot \text{ yr}^{-1}$  for FU Ori. Note that this is a current estimate, as the object has faded at optical wavelengths by more than a magnitude (e.g., Kenyon et al. 2000). We take a range of  $2.8 - 3.8 \times 10^{-5} M_\odot \text{ yr}^{-1}$  for FU Ori and  $7 - 11 \times 10^{-5} M_\odot \text{ yr}^{-1}$  for V1883 Ori from Liu et al. (2022). For Gaia 17bpi, Rodriguez & Hillenbrand (2022) (RH22) estimated  $\dot{M} \sim 0.9 - 6 \times 10^{-7} M_\odot \text{ yr}^{-1}$ . Then Figure 5 suggests triggering at  $\sim 2 - 1$ , and  $\sim 0.1$  au for V1883 Ori, FU Ori, and Gaia 17bpi, respectively.

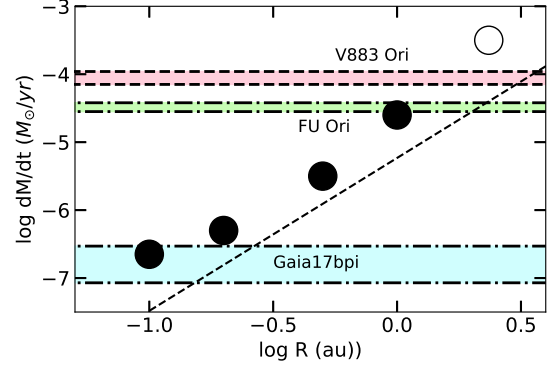


**Figure 5.** Dependence of the central mass accretion rate, estimated at the “plateau” value immediately after the main spike (see Figure 3), as a function of radius for the model sequence displayed in Figure 4. The dashed line is given by equation 8. We use large dots to indicate that the precise values depend on exactly the time at which the (varying) accretion rate is measured. The ranges of estimated accretion rates for Gaia 17 bpi are taken from Rodriguez & Hillenbrand (2022) (RH22), but multiplied by a factor of two to account for the difference between their assumption of  $0.6 M_\odot$  for the central mass in contrast to the  $0.3 M_\odot$  of the present calculation (the disc luminosity and temperature depend upon the joint product of  $M_* \dot{M}$ ). The ranges for FU Ori and V883 Ori are the best values from RH22 and Liu et al. (2022); these probably underestimate the true uncertainties but are used to avoid overlap (see discussion in §4).

Using equation 6, one can make a crude estimate of the expected mass accretion rate using the formula for a steady disc,

$$\begin{aligned} \dot{M}_i &= 3\pi\alpha c_s^2 \Sigma \Omega^{-1} \\ &= 2.2 \times 10^{-5} (\alpha_{-1} \kappa_i)^{1/2} M_{0.3}^{-3/4} R_t^{9/4} T_i^{5/2} M_\odot \text{ yr}^{-1}, \end{aligned} \quad (7)$$

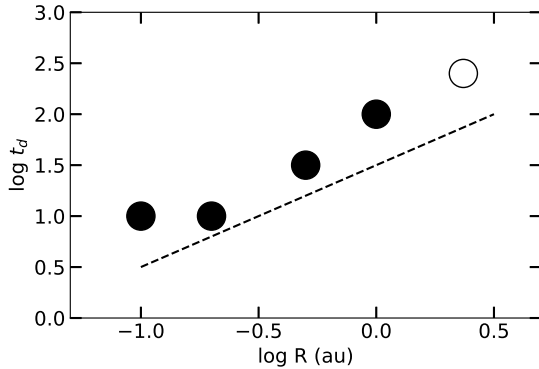
where  $R_t$  is the radius in au at which the perturbation was placed. Figure 5 shows that equation 8 again reproduces the radial scaling, but lower than predicted by equation 8; this is as expected from the results for the critical  $\Sigma$  (§3.3. These are minimum accretion rates due to the assumption of a flat inner surface density distribution;  $\dot{M}$  can be a few times higher for models with increasing surface densities with decreasing radius, as discussed later in §4.2.

Figure 6 shows decay timescales for the models. Relating this simply to a viscous time is complicated because of the nature of the central temperature distribution, with a hot inner region and a colder outer disc, although one expects this to depend approximately inversely with  $\alpha$ . As indicated by the dashed line, the dependence of the decay time on radius is found to be roughly proportional to  $R$ .

In the one-dimensional outburst models by Zhu et al. (2010a); Bae et al. (2013), mass infall to the outer disc is transported inward by gravitational instabilities, eventually resulting in enough heating to trigger the MRI at a radius  $\sim 3$  au; The results in Figure 5 are roughly consistent with this triggering radius. The observed rate of decay of FU Ori,  $\sim 0.015 \text{ mag yr}^{-1}$  in the B and V bands (Kenyon et al. 2000), is reasonably consistent with the predicted  $\sim 100 \text{ yr}$  decay timescale (Figure 6).

## 4 DISC EVOLUTION AND LIGHT CURVES

A major motivation in constructing simple time-dependent accretion models is to make comparisons with observed light curves. Following RH22, the spectral energy distribution for each model at each snapshot in time (taken at 1/2 year intervals) was calculated



**Figure 6.** Approximate decay timescales of the central mass accretion rates for the models, defined as the time taken to decay by a factor of two from the plateau immediately after the initial spike in  $\dot{M}$ , as a function of the radius at which the initial perturbation was applied. Using the entire length of the outburst instead leads to similar results, with timescales larger by about 30-40%. The dashed line denotes  $t_d \propto R$  for comparison.

from the sum of the spectra of each annulus taken from a model atmosphere with the same effective temperature. We used the BT-NextGen<sup>2</sup> (AGSS2009) calculations (Allard et al. 2011, 2012) for temperatures between 15,000 K and 2700 K, setting  $\log g = 1$  as appropriate for discs (see, e.g. Liu et al. 2022). For lower temperatures between 1400 and 2700 K we use the BT-Settl<sup>3</sup> (AGSS2009) models. For these temperatures we take the lowest surface gravity available in the model set,  $\log g = 3.5$  (Liu et al. 2022). At temperatures below 1400 K we assume that dust forms a featureless continuum and that the resulting spectrum is that of a blackbody. In all cases we assume an inclination of  $60^\circ$  to the line of sight.

We found it unnecessary to keep the full (very high) spectral resolution of the atmosphere models. Following RH22, We include the flux of a central star of a given radius and effective temperature that radiates as the corresponding BT-NextGen model.

For comparison with observations that are reddened by interstellar extinction, we used the PyAstronomy module Unred<sup>4</sup> with the extinction correction for  $R_V = 3.1$  as defined in Fitzpatrick (1999). Supplying in a negative value for the color excess  $E(B-V)$ , we were then able to add in wavelength-dependent extinction.

To facilitate comparison with observations, we computed magnitudes for the GAIA G, WISE W1, WISE W2, CTIO V, and the 2MASS J, H, and K filters (Cutri et al. 2003). We obtained transmission-wavelength data from the SVO Filter Profile Service<sup>5</sup> as defined in (Rodrigo et al. 2012; Rodrigo & Solano 2020). The GAIA G magnitudes were computed with the method presented by Evans et al. (2018).

In the following we compute light curves and spectral energy distributions (SEDs) of models exhibiting small and large outbursts. We compare the results with observations of Gaia 17bpi and FU Ori that may be taken as representative of these two cases. Our goal is not to model the data precisely, which is not possible in any case given the limitations of the simulations, but to see the extent to which simple models can explain the overall outburst behaviors.

#### 4.1 Weak outburst: Gaia 17bpi

For purposes of comparison to the observed light curves of Gaia 17bpi and to previous modeling, we fix the distance as 1.27 kpc (Hillenbrand et al. 2018) and adopt the visual extinction of  $A_V = 3.5$  as estimated by RH22. The high-state accretion rate of  $\sim 1 - 3 \times 10^{-7} M_\odot \text{ yr}^{-1}$  estimated by RH22 assumed a central mass of  $\sim 0.6 M_\odot$ . For these models, where we have instead assumed  $M_* = 0.3 M_\odot$ , the corresponding accretion rate would be  $\sim 2 - 6 \times 10^{-7} \times M_\odot \text{ yr}^{-1}$ , because the product  $\dot{M} M_*$  enters in to both the luminosity and maximum disc temperature of a steady optically-thick disc. For the final model we assume an inner radius of 0.003 au to correspond more closely to the (very small) stellar radius of  $\sim 0.4 R_\odot$  of RH22. (We had numerical problems going to smaller radii.) A viscosity parameter of  $\alpha = 0.1$  was assumed. RH22 assumed a central star mass of  $0.6 M_\odot$ , but we find no significant difference in the outburst changing mass by a factor of two.

Figure 5 indicates that the temperature perturbation should be located interior to about 0.2 au, and that a minimum surface density should be  $\sim 2000 \text{ g cm}^{-2}$ . Consistent with these expectations, the initial condition of our final model shown in the left panel of Figure 7 exhibits a temperature perturbation centered at 0.09 au at a region of constant surface density  $\Sigma = 2000 \text{ g cm}^{-2}$ . The surface density is strongly depleted inside of 0.05 au to avoid having the innermost regions go into outburst first, resulting in an outside-in burst (§3.1). We interpret our evacuated inner region as corresponding to magnetospheric truncation. The falloff of  $\Sigma$  beyond 1.5 au was introduced in a (failed) attempt to make the WISE fluxes smaller, but it has little effect on the outburst. (Further discussion of how we arrived at this model, along with illustrations of the effect of changing various parameters, is presented in the Appendix.)

The disc evolution shown in Figure 7 is similar to that shown in Figures 1 and 2. The onset of a high viscosity results in the propagation of mass inward in a sharp spike (see middle panel), along with an outward pileup to conserve angular momentum, and a significant minimum in the surface density in between. During this phase the outburst would be detected only at infrared wavelengths. As the accretion front reaches the star, the central temperature jumps up and reaches very high values due to thermal instability (see right panel).

As shown in Figure 8, the accretion rate plateaus at a value  $\sim 3 \times 10^{-7} M_\odot \text{ yr}^{-1}$ , as expected. The peak temperature in the inner disc is  $\sim 6000$  K, somewhat cooler than the  $\sim 7600$  K estimated by RH22. We note that our models employ a flow-through inner boundary condition, and so they do not show the turnover of the effective temperature that results in steady disc models with a zero-torque boundary condition.

Figure 9 shows the resulting light curves, with the data taken from the Cambridge Photometry Calibration Server<sup>6</sup> and the NEOWISE-R Single Exposure Source Table<sup>7</sup> with the time offset to provide a reasonable match to the NEOWISE magnitudes. The overall behavior is comparable to the observations, except that the optical rise is much faster and sharper than seen in the observations, and the plateau phase is too faint by a little more than one magnitude. Within the context of our models, there is really no way of avoiding a sharp optical peak; the onset of the temperature perturbation always results in a snowplow making a very large, concentrated surface density spike. Note that the immediate drop in the light curves is due to the initial conditions at the very inner edge of the disc which are not consistent

<sup>2</sup> <http://svo2.cab.inta-csic.es/theory/newov2/index.php?models=bt-nextgen-agss2009>

<sup>3</sup> <http://svo2.cab.inta-csic.es/theory/newov2/index.php?models=bt-settl-agss>

<sup>4</sup> <https://pyastronomy.readthedocs.io/en/latest/pyastronomy/aslDoc/units/units.html>

<sup>5</sup> <http://svo2.cab.inta-csic.es/theory/fps/>

<sup>7</sup> <https://irsa.ipac.caltech.edu/>

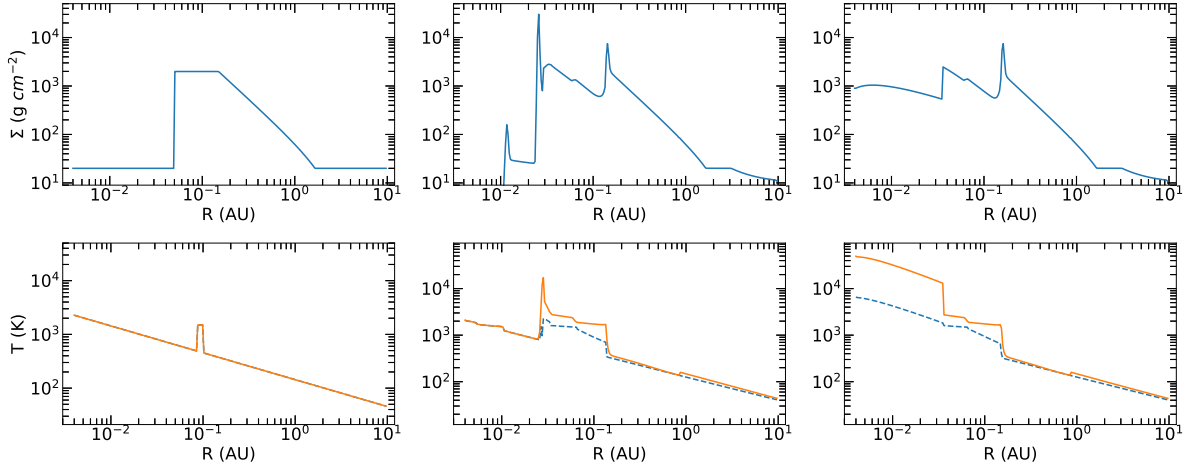


**Figure 7.** Evolution of an outburst model to compare with observations of Gaia17bpi. The upper panels show the the surface density structure and temperature at three times; the initial condition, the development of the outburst, and the structure at peak accretion rate. The dashed and solid curves show the surface (effective) temperature and the central temperature, respectively. From left to right, the plots outline structure occurring at 0, 4, and 5 years from the start of the model.

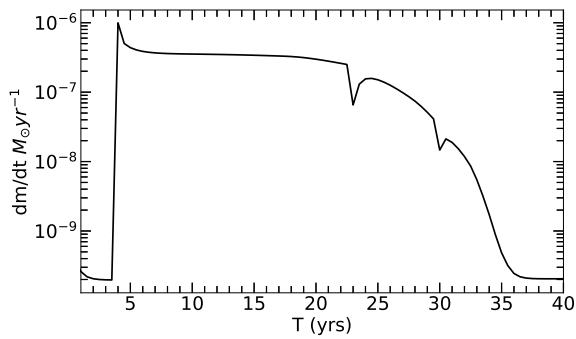


**Figure 8.** Central accretion rate vs. time for the model shown in Figure 7.

with steady state. These produce a slightly higher accretion rate at first, which dies out quickly.

We were able to increase the optical flux with the same structural model but doubling the surface density of the flat region, to  $\Sigma = 4000 \text{ g cm}^{-2}$ . As shown in Figure 10, this results in much better agreement with the optical light curve, with a peak temperature of  $\sim 7300 \text{ K}$ , but now W1 and W2 are too bright by about one magnitude. In general we were unable to find a model that substantially changed the infrared/optical flux ratio. As discussed in the Appendix, there is a feature in the model temperature distribution that differs from the simple  $T \propto R^{-3/4}$  steady disc solution, and this can account for part of the discrepancy. Alternatively, it may be possible that the actual extinction is lower than  $A_V = 3.5$  (see discussion in Hillenbrand et al. 2018), or possibly that the IR-optical extinction law is flatter than the standard (Wang & Chen 2019). Finally, of course, there may be limitations of our simple treatment of time-dependent disc accretion.

A brief exploration of other parameter choices is presented in the Appendix. As shown there, the time lag between infrared and optical outbursts is somewhat sensitive to the position of the temperature perturbation. Moreover, values of the alpha parameter that are three times smaller or larger lead to lag times between the infrared and optical outbursts that are much too large or too small respectively.

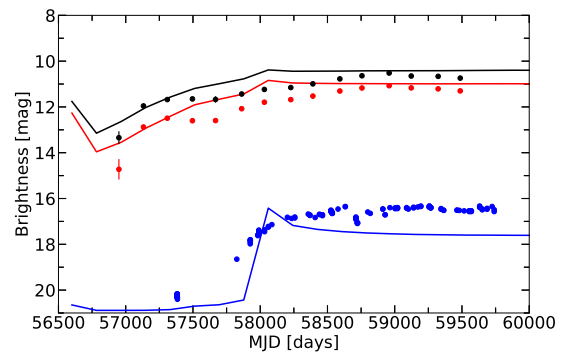


**Figure 9.** Model light curves resulting from the initial conditions shown in Figure 7, compared with photometry of Gaia 17bpi. The black and red dots and curves are the WISE W1 and W2 magnitudes and model results, respectively, while the blue dots and curve are the Gaia G band photometry and corresponding model magnitudes. The time  $t = 0$  in Figure 8 corresponds to MJD = 56600. The initial drop in the infrared light curves is due to transient accretion at the inner edge of the disk that dies away rapidly (see text). The rise time of the optical light curve is unresolved at the plotted 0.5 year sampling. A test run with higher resolution sampling indicates that the true rise is about 1 month (the individual time steps of the calculation are much shorter).

Overall, we conclude that the propagation of the outburst can be explained in with  $\alpha = 0.1$ , in agreement with the estimate of Liu et al. (2022).

#### 4.2 Strong, FU Ori-like outburst

To simulate a large FU Ori-like outburst, we constructed a model with an initial condition similar to that in Figures 1 and 2 with the temperature perturbation placed at 1 au. This is similar to our previous models of FU Ori outbursts resulting from continuing infall to the disc, which generates GI turbulent heating and subsequently MRI activation at radii  $\sim 3 \text{ au}$  (Zhu et al. 2009, 2010b; Bae et al. 2013, 2014). However, in this case the outburst is triggered by hand rather than by GI.

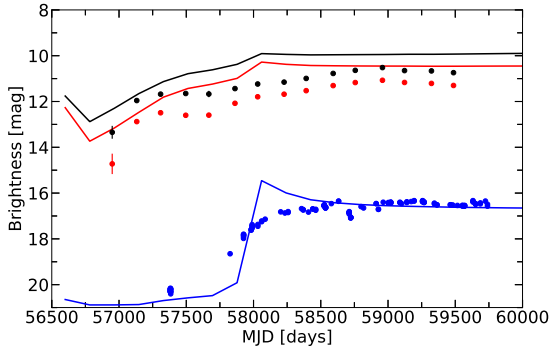


**Figure 10.** Light curves for a model with the same parameters as those in Figures 7, 8, and 9, except with twice the flat region surface density. The dots and curves are as in Figure 9.

In contrast to the model shown in Figures 1 and 2, we decided to explore the effect of a rising surface density  $\Sigma \propto R^{-1/2}$  interior to the temperature perturbation (see Figure 11). (A steeper dependence on radius results in triggering the MRI at very small radii, resulting in an inside-out burst). We also impose an outer surface density distribution decreasing as  $\Sigma \propto R^{-7/4}$ . This is done to avoid a gravitationally-unstable outer disc; with  $T \propto R^{-1/2}$ , the Toomre parameter  $Q \propto T^{1/2}\Omega/\Sigma$  remains constant (and sufficiently large).

The evolution of the temperature and surface density is very similar to the previous model. The main difference is that the higher inner surface density produces accretion rates that are about 2-3 times larger during the plateau phase, with higher accretion rates and a longer outburst (compare Figure 12 with Figure 3).

As in the case of Gaia 17bpi, the light curves (Figure 13) show that the infrared outburst precedes the optical event, as the accretion wave moves inward and the disc temperatures rise. However, in this case the lag time is much larger, with the infrared rise starting about 40 years before the optical brightening, consistent with a longer timescale for an outburst starting at much larger radii. The mean propagation speed of the accretion wave is  $v_p \sim 1 \text{ au}/40 \text{ yr} \sim 0.1 \text{ km s}^{-1}$ . With a sound speed at 1500 K of  $2.3 \text{ km s}^{-1}$ ,  $v_p$  is of the order  $\alpha c_s$ , as expected from  $\alpha$ -disc theory (e.g., Bell & Lin 1994). The actual propagation is not steady, but speeds up with time as the disc temperature rises.

## 5 DISCUSSION

### 5.1 Small outbursts: Gaia 17bpi

Our models indicate that small outbursts can be explained by MRI activation of low surface density inner discs. These are very unlikely to be produced by GI in discs, though other mechanisms (see Introduction) remain. GI triggering at large radii results in high accretion rates. These large outbursts, if MRI-driven, are likely to be confined to disc radii within a few AU, as the required trapping of heat would imply extremely large surface densities that would be so gravitationally-unstable that they would likely evolve on dynamical timescales. Note that we adopted the lowest surface density at each radius that sustains the MRI; larger surface densities would produce larger accretion rates.

In the case of Gaia 17bpi, we imposed a low surface density in the innermost disc prior to outburst, attributing that to the usual magnetospheric truncation. However, we cannot achieve the necessary peak optical spectral type or effective temperature (given the accretion rate

or luminosity) unless the magnetosphere is crushed or otherwise absent, with an inner radius close to the  $\sim 0.65 R_\odot$  estimated by RH22. The absence of the usual broad optical emission lines characteristic of magnetospheric flows supports the absence of disc truncation.

Standard theory predicts that the magnetospheric truncation radius is given by (e.g., Königl 1991)

$$R_m = \beta B^{4/7} R^{12/7} \dot{M}^{-2/7} (2GM)^{-1/7}, \quad (9)$$

where  $B$  is the surface (dipolar) field,  $R$  and  $M$  are the stellar radius and mass respectively, and  $\dot{M}$  is the mass accretion rate. The magnetosphere is crushed when  $R_m = R$ , or

$$\begin{aligned} \dot{M}_c &= \beta^{7/2} B^2 R^{5/2} (GM)^{-1/2} \\ &= 10^{-6} \beta_{0.5}^{7/2} B_{1.5}^2 R_{1.5}^{5/2} (GM_{0.5})^{-1/2} M_\odot \text{ yr}^{-1}, \end{aligned} \quad (10)$$

where the fiducial values are  $\beta_{0.5} = 0.5$ ,  $B_{1.5} = 1500 \text{ G}$ ,  $R_{1.5} = 1.5 R_\odot$ , and  $M_{0.5} = 0.5 M_\odot$ . The parameter  $\beta$  is poorly known; we take a fiducial value of 0.5 (Königl 1989), which with the other fiducial parameters yields a typically estimated magnetospheric radius of  $\sim 5 R_*$  for a median T Tauri accretion rate of  $10^{-8} M_\odot \text{ yr}^{-1}$  and a stellar mass and radius of  $0.5 M_\odot$  and  $2 R_\odot$ . Thus, for the classical FU Ori objects, with accretion rates  $\geq 10^{-5} M_\odot \text{ yr}^{-1}$ , one would expect the magnetosphere to be suppressed, consistent with the observed lack of magnetospheric emission lines.

At first, it seems surprising that the low accretion rate implied for Gaia 17bpi can crush the magnetosphere. However, RH22 estimated a remarkably small inner disc radius for this object  $\sim 0.36 - 0.48 R_\odot$ . Assuming the other fiducial parameters in equation 11, a stellar radius of  $0.5 R_\odot$  yields  $\dot{M}_c \sim 6 \times 10^{-8} M_\odot \text{ yr}^{-1}$ . In other words, a fixed magnetic field strength on a much smaller star yields a much smaller magnetic moment and less magnetospheric resistance to accretion.

### 5.2 Large, FU Ori-like outbursts

Our results are similar to those of our previous models of GI triggering of the MRI in discs on scales of order 1-3 au (Zhu et al. 2010b; Bae et al. 2013, 2014). The simulations predict a much sharper optical rise in brightness compared with observations. This may be an artifact of our assumption of axisymmetry and neglect of convection (see Zhu et al. (2010a)). Moreover, the present treatment of MRI activation is of course schematic; it may not capture the real physics of the onset of magnetic turbulent viscosity from an inert state.

The innermost disc effective temperatures that we predict tend to be larger than typically observed in outbursts ( $\sim 10,000 \text{ K}$  vs.  $\sim 6000 \text{ K}$ ). Again, the flow-through inner boundary adopted here means that there is no turn-over in the disc temperature distribution at small radii characteristic of the steady-disc solution, which assumes a zero-torque boundary condition. We also have not taken into account any possible energy loss via the ejection of winds, which would reduce disc temperatures (Zhu et al. 2020). Peak temperatures are also sensitive to the inner disc radius for a given accretion rate and stellar mass. For example, in the case of FU Ori, SED modeling suggests that the inner radius must be  $\sim 3 - 4 R_\odot$  (Hartmann & Kenyon 1996), which is considerably larger than the typical radii of  $0.6 M_\odot$  pre-main sequence stars. It has been suggested that this is the result of advection of large amounts of thermal energy into the central star, increasing its radius (Baraffe et al. 2012). On the other hand, there are outbursting objects whose optical spectra seem to be of higher effective temperature and/or weaker or absent absorption lines, or exhibit some composite signatures of "hot" and "cool" spectra (Hillenbrand et al. 2019a,b). High accretion rate objects with higher temperatures also tend to have very strong wind emission lines, which makes them harder to classify and/or interpret.

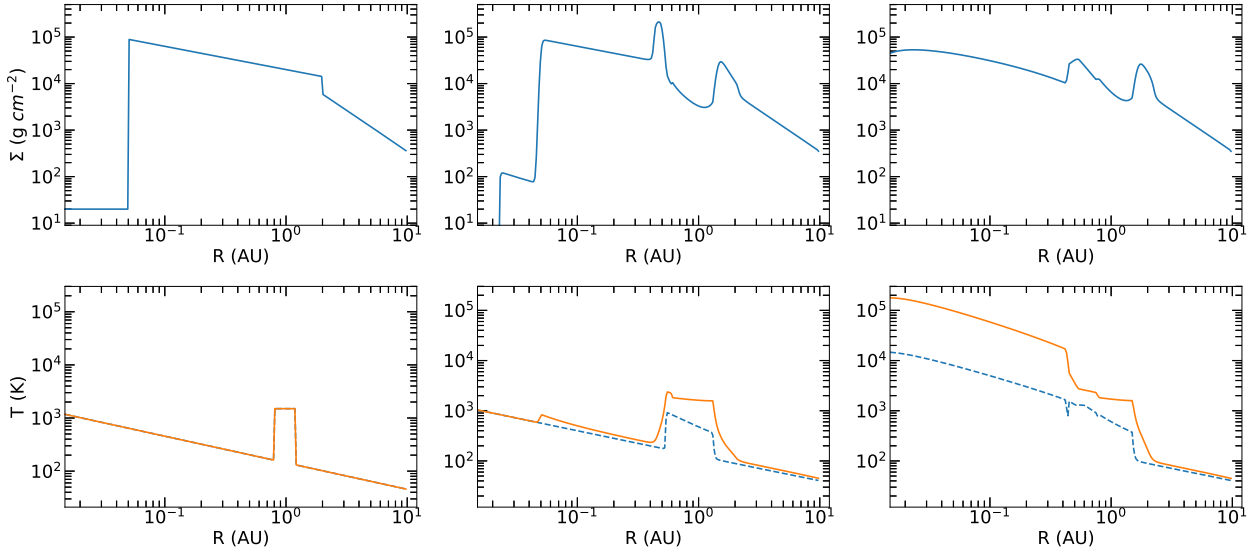


**Figure 11.** Evolution of an outburst model similar to FU Ori, showing the surface density structure and temperature at three times; the initial condition, the development of the outburst, and the structure at peak accretion rate. The dashed and solid curves show the surface (effective) temperature and the central temperature, respectively. From left to right, the structures are shown at 0, 70, and 95 years after the start of the model.

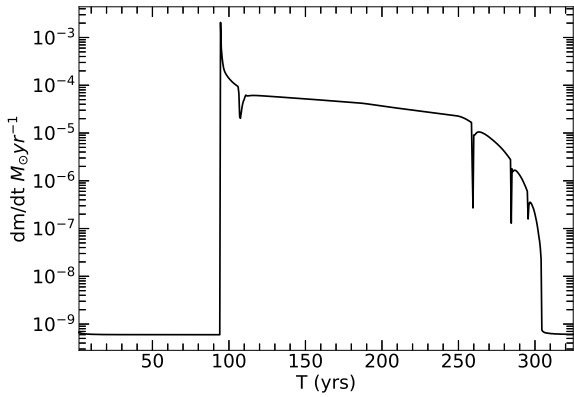


**Figure 12.** Accretion rate vs. time for the model in Figure 11.

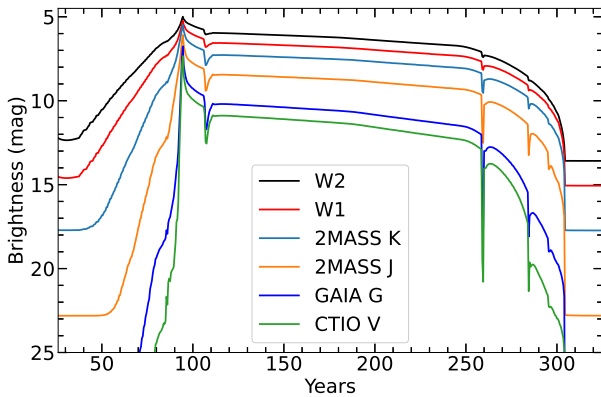


**Figure 13.** Light curves for a model FU Ori outburst. The light curves, from top to bottom, correspond in order to that shown in the legend.

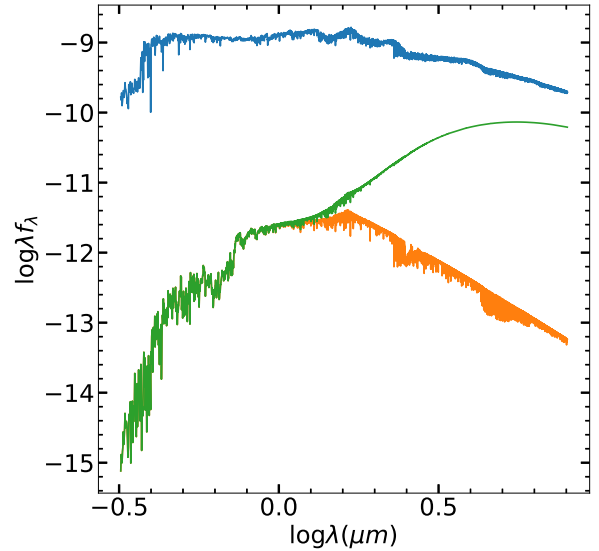


**Figure 14.** SEDs of FU Ori-type model, shown at  $t = 70$  and  $100$  yr (see Figure 13). At  $t = 70$  yr, the SED (green curve) is dominated by the stellar photosphere out to almost  $\lambda = 2\mu\text{m}$ , but exhibits a large infrared excess compared to the stellar emission (orange spectrum). (The green curve overlaps the orange exactly at shorter wavelengths.) The upper (blue) curve shows the spectrum in full outburst at  $t = 160$  yr, similar to that observed in FU Ori.

The most important result of our latest simulations of large-scale outbursts is the finding that, assuming  $\alpha$  parameters similar to those estimated for Gaia 17bpi, infrared outbursts can be detected many years or even decades in advance of optical bursts, depending upon where the outburst is triggered and the effective value of  $\alpha$ . This assumes outside-in propagation; V1515 Cyg shows a slow optical rise that may suggest inside-out triggering, in which case the optical and infrared rises will occur roughly simultaneously (e.g., Bell et al. 1995). In this context, the recent suggestion by Nayakshin et al.

(2023) that FU Ori outbursts are fueled by evaporation of hot Jupiters close to the central star would predict that the infrared light curve would not exhibit much lag behind the optical rise. Multi-wavelength observations can thus provide a definitive test of the two different scenarios.

Another possible test of the outside-in large outburst picture would be the observation of large far-infrared excesses in objects that are in optical quiescence. As shown in Figure 14, a large accretion rate burst originating at  $\sim 1$  au would have a very large far-IR precursor. Distinguishing this behavior from other possibilities, such as radiation from a protostellar envelope, or an unresolved luminous companion, such as in Z CMa (Koresko et al. 1991; Hinkley et al. 2013), can be difficult but still may be worthy of consideration.

As noted in the Introduction, many theoretical simulations of FU Ori-type outbursts have been conducted, employing different triggering mechanisms. It is difficult to consider the implications of most of these studies for our work, because they generally assume inner radii far larger than considered here. For example, the Kadam et al. (2020) study employs an inner radius of 0.42 au, and most of the evolution and emission that we calculate arises inside that boundary. This is true even of our own previous work (for example, the inner radius is 0.2 au in Bae et al. 2014).

Our findings suggest that infrared surveys, for example as might be provided by the *Roman Space Telescope* and other facilities, could provide crucial insights into the physics of outbursts. Whether currently-detected variables in the infrared (e.g. Fischer et al. 2019, 2022) will later have optical bursts remains to be seen. Further optical detections of bursts will obviously motivate searches for prior infrared detections.

## 6 SUMMARY

Using simple time-dependent models of disc outbursts, buttressed by basic theoretical considerations, we find that activation of the MRI can account for many features of the diversity of observed accretion events. short-lived, relatively low accretion rate events probably result from triggering in the inner disc, and can occur at low surface densities, comparable to or smaller than the minimum mass solar nebula, and thus are very unlikely to result from MRI triggering by gravitational instability. We find that the time lag between the infrared precursor of the outburst of Gaia 17bpi and the optical rise indicates a rate of inward propagation consistent with  $\alpha \sim 0.1$ . We further find that larger outbursts, which must arise farther out in massive discs, exhibit infrared precursors decades before optical outbursts, raising the possibility of detecting bursts early enough to study the central star effectively, along with providing insights into accretion physics. These results emphasize the need for continued wide-field infrared monitoring, such as the VVV program (Contreras Peña et al. 2014; Lucas et al. 2017, 2020; Park et al. 2021; Guo et al. 2022) and NEOWISE (Park et al. 2021; Zakri et al. 2022; Contreras Peña et al. 2023) to complement the expected growth in optical outburst detections over the next several years from all-sky surveys such as from the *Vera Rubin Observatory*. Finally, three-dimensional non-ideal magnetohydrodynamic simulations will be needed to take full advantage of the observational results.

## ACKNOWLEDGEMENTS

We thank Lynne Hillenbrand for help with obtaining more recent light curves of Gaia 17bpi and an anonymous referee for a very

helpful report. This work was supported in part by the University of Michigan. Our research has made use of the Spanish Virtual Observatory (<https://svo.cab.inta-csic.es>) project funded by MCIN/AEI/10.13039/501100011033/ through grant PID2020-112949GB-I00. This work has made use of data from the European Space Agency (ESA) mission *Gaia* (Gaia Collaboration et al. 2016, 2022); (<https://www.cosmos.esa.int/gaia>) processed by the *Gaia* Data Processing and Analysis Consortium (DPAC, <https://www.cosmos.esa.int/web/gaia/dpac/consortium>). Funding for the DPAC has been provided by national institutions, in particular the institutions participating in the *Gaia* Multilateral Agreement. This publication also makes use of data products from the Near-Earth Object Wide-field Infrared Survey Explorer (NEOWISE) (Mainzer et al. 2014; Cutri et al. 2015), which is a joint project of the Jet Propulsion Laboratory/California Institute of Technology and the University of Arizona. NEOWISE is funded by the National Aeronautics and Space Administration.

Software: PyAstronomy (Czesla et al. 2019), Spectres (Carnall 2017), and Matplotlib (Hunter 2007).

## DATA AVAILABILITY

The models and associated data will be provided upon reasonable request to the authors.

## REFERENCES

- Allard F., Homeier D., Freytag B., 2011, in Johns-Krull C., Browning M. K., West A. A., eds, *Astronomical Society of the Pacific Conference Series* Vol. 448, 16th Cambridge Workshop on Cool Stars, Stellar Systems, and the Sun. p. 91 ([arXiv:1011.5405](https://arxiv.org/abs/1011.5405))
- Allard F., Homeier D., Freytag B., 2012, *Philosophical Transactions of the Royal Society of London Series A*, 370, 2765
- Armitage P. J., Livio M., Pringle J. E., 2001, *MNRAS*, 324, 705
- Audard M., et al., 2014, in Beuther H., Klessen R. S., Dullemond C. P., Henning T., eds, *Protostars and Planets VI*. p. 387 ([arXiv:1401.3368](https://arxiv.org/abs/1401.3368)), [doi:10.2458/azu\\_uapress\\_9780816531240-ch017](https://doi.org/10.2458/azu_uapress_9780816531240-ch017)
- Bae J., Hartmann L., Zhu Z., Gammie C., 2013, *ApJ*, 764, 141
- Bae J., Hartmann L., Zhu Z., Nelson R. P., 2014, *ApJ*, 795, 61
- Bai X.-N., Stone J. M., 2013a, *ApJ*, 767, 30
- Bai X.-N., Stone J. M., 2013b, *ApJ*, 769, 76
- Bai X.-N., Ye J., Goodman J., Yuan F., 2016, *ApJ*, 818, 152
- Baraffe I., Vorobyov E., Chabrier G., 2012, *ApJ*, 756, 118
- Bell K. R., Lin D. N. C., 1994, *ApJ*, 427, 987
- Bell K. R., Lin D. N. C., Hartmann L. W., Kenyon S. J., 1995, *ApJ*, 444, 376
- Bell K. R., Cassen P. M., Wasson J. T., Woolum D. S., 2000, in Mannings V., Boss A. P., Russell S. S., eds, *Protostars and Planets IV*. p. 897
- Bouvier J., et al., 2020, *A&A*, 636, A108
- Carnall A. C., 2017, *arXiv e-prints*, p. arXiv:1705.05165
- Ciesla F. J., 2007, *Science*, 318, 613
- Ciesla F. J., 2010, *Icarus*, 208, 455
- Contreras Peña C., et al., 2014, *MNRAS*, 439, 1829
- Contreras Peña C., et al., 2023, *MNRAS*, 521, 5669
- Cutri R. M., et al., 2003, *VizieR Online Data Catalog*, p. II/246
- Cutri R. M., et al., 2015, *Explanatory Supplement to the NEOWISE Data Release Products*, *Explanatory Supplement to the NEOWISE Data Release Products*, <A href="http://wise2.ipac.caltech.edu/docs/release/neowise/expSUP">http://wise2.ipac.caltech.edu/docs/release/neowise/expSUP</A>
- Czesla S., Schröter S., Schneider C. P., Huber K. F., Pfeifer F., Andreasen D. T., Zechmeister M., 2019, *PyA: Python astronomy-related packages* (ascl:1906.010)
- D’Alessio P., Calvet N., Hartmann L., 2001, *ApJ*, 553, 321

Desch S. J., Turner N. J., 2015, *ApJ*, **811**, 156  
 Evans D. W., et al., 2018, *A&A*, **616**, A4  
 Fischer W. J., Safron E., Megeath S. T., 2019, *ApJ*, **872**, 183  
 Fischer W. J., Hillenbrand L. A., Herczeg G. J., Johnstone D., Kóspál Á., Dunham M. M., 2022, arXiv e-prints, p. arXiv:2203.11257  
 Fitzpatrick E. L., 1999, *PASP*, **111**, 63  
 Flaherty K. M., Hughes A. M., Rosenfeld K. A., Andrews S. M., Chiang E., Simon J. B., Kerzner S., Wilner D. J., 2015, *ApJ*, **813**, 99  
 Flaherty K., et al., 2020, *ApJ*, **895**, 109  
 Forgan D., Rice K., 2010, *MNRAS*, **402**, 1349  
 Gaia Collaboration et al., 2016, *A&A*, **595**, A1  
 Gaia Collaboration et al., 2022, arXiv e-prints, p. arXiv:2208.00211  
 Gehrig L., Steiner D., Vorobyov E. I., Güdel M., 2022, *A&A*, **667**, A46  
 Gravity Collaboration et al., 2020, *Nature*, **584**, 547  
 Guo Z., et al., 2022, *MNRAS*, **513**, 1015  
 Hartmann L., Bae J., 2018, *MNRAS*, **474**, 88  
 Hartmann L., Kenyon S. J., 1996, *ARA&A*, **34**, 207  
 Hartmann L., Herczeg G., Calvet N., 2016, *ARA&A*, **54**, 135  
 Herbig G. H., 1977, *ApJ*, **217**, 693  
 Hillenbrand L. A., et al., 2018, *ApJ*, **869**, 146  
 Hillenbrand L. A., Reipurth B., Connelley M., Cutri R. M., Isaacson H., 2019a, *AJ*, **158**, 240  
 Hillenbrand L. A., et al., 2019b, *ApJ*, **874**, 82  
 Hinkley S., et al., 2013, *ApJ*, **763**, L9  
 Hubeny I., 1990, *ApJ*, **351**, 632  
 Hunter J. D., 2007, *Computing in Science & Engineering*, **9**, 90  
 Kadam K., Vorobyov E., Regály Z., Kóspál Á., Ábrahám P., 2020, *ApJ*, **895**, 41  
 Kenyon S. J., Hartmann L. W., Kolotilov E. A., 1991, *PASP*, **103**, 1069  
 Kenyon S. J., Kolotilov E. A., Ibragimov M. A., Mattei J. A., 2000, *ApJ*, **531**, 1028  
 Kolotilov E. A., Kenyon S. J., 1997, *Information Bulletin on Variable Stars*, **4494**, 1  
 Königl A., 1989, *ApJ*, **342**, 208  
 Kopatskaya E. N., Kolotilov E. A., Arkharov A. A., 2013, *MNRAS*, **434**, 38  
 Koresko C. D., Beckwith S. V. W., Ghez A. M., Matthews K., Neugebauer G., 1991, *AJ*, **102**, 2073  
 Larson R. B., 1983, *Rev. Mex. Astron. Astrofis.*, **7**, 219  
 Liu H., et al., 2022, *ApJ*, **936**, 152  
 Lodato G., Clarke C. J., 2004, *MNRAS*, **353**, 841  
 Lucas P. W., et al., 2017, *MNRAS*, **472**, 2990  
 Lucas P. W., et al., 2020, *MNRAS*, **499**, 1805  
 Mainzer A., et al., 2014, *ApJ*, **792**, 30  
 Nayakshin S., Lodato G., 2012, *MNRAS*, **426**, 70  
 Nayakshin S., Owen J. E., Elbakyan V., 2023, arXiv e-prints, p. arXiv:2305.03392  
 Park W., et al., 2021, *ApJ*, **920**, 132  
 Rodrigo C., Solano E., 2020, in XIV.0 Scientific Meeting (virtual) of the Spanish Astronomical Society. p. 182  
 Rodrigo C., Solano E., Bayo A., 2012, SVO Filter Profile Service Version 1.0, IVOA Working Draft 15 October 2012, doi:10.5479/ADS/bib/2012ivoa.rept.1015R  
 Rodríguez A. C., Hillenbrand L. A., 2022, *ApJ*, **927**, 144  
 Semkov E., Ibrayamov S., Peneva S., 2021, *Symmetry*, **13**, 2433  
 Szabó Z. M., et al., 2022, *ApJ*, **936**, 64  
 Szegedi-Elek E., et al., 2020, *ApJ*, **899**, 130  
 Vorobyov E. I., Basu S., 2006, *ApJ*, **650**, 956  
 Vorobyov E. I., Basu S., 2010, *ApJ*, **719**, 1896  
 Vorobyov E. I., Elbakyan V. G., Takami M., Liu H. B., 2020, *A&A*, **643**, A13  
 Vorobyov E. I., Elbakyan V. G., Liu H. B., Takami M., 2021, *A&A*, **647**, A44  
 Wang S., Chen X., 2019, *ApJ*, **877**, 116  
 Zakri W., et al., 2022, *ApJ*, **924**, L23  
 Zhu Z., Hartmann L., Calvet N., Hernandez J., Muzerolle J., Tannirkulam A.-K., 2007, *ApJ*, **669**, 483  
 Zhu Z., Hartmann L., Gammie C., 2009, *ApJ*, **694**, 1045  
 Zhu Z., Hartmann L., Gammie C. F., Book L. G., Simon J. B., Engelhard E., 2010a, *ApJ*, **713**, 1134  
 Zhu Z., Hartmann L., Gammie C., 2010b, *ApJ*, **713**, 1143

Zhu Z., Jiang Y.-F., Stone J. M., 2020, *MNRAS*, **495**, 3494

## APPENDIX

Our first attempt at a model for Gaia 17bpi, assuming with  $\alpha = 0.1$  is shown in Figure 15. The inner disc radius is set at 0.005 au ( $\sim 1R_{\odot}$ ). The surface density is a constant  $2000 \text{ g cm}^{-2}$  between 0.05 and 2 au, but with a strong depletion inside of 0.05 au. This is to avoid having the innermost regions go into outburst first, resulting in an outside-in burst §3.1. We interpret our evacuated inner region as corresponding to magnetospheric truncation. The falloff of  $\Sigma$  at large radii is intended to prevent GI, but in any event the outburst cycle is not affected by this structure. The imposed temperature perturbation is centered at 0.10 au. In summary, this initial structure is very similar to that used for our “final” Gaia 17bpi model (Figure 7. except the high surface density region extends to larger radii. The resulting evolution in Figures 15, 16, and 17 is very similar to that shown in Figures 7, 8, and 9.

Figure 17 shows a slightly larger lag time between infrared and optical bursts than observed. The difference with the results shown in Figure 9 is that in the latter case the temperature perturbation was centered at 0.09 au instead of 0.10 au. However, the lag time is much more sensitive to the adopted alpha parameter. In Figure 18 we show the effects of changing the  $\alpha$  parameter on the lag time between infrared and optical light curves. (We reduced the surface density for the large viscosity case because we wanted to keep a similar accretion rate, and  $\dot{M} \propto \alpha \Sigma$ .) It is clear that  $\alpha = 0.3$  yields very little lag time between the infrared and optical light curves, while  $\alpha = 0.03$  results in a much longer lag than observed.

Another issue is that the WISE fluxes are too bright relative while the G fluxes are low. We lowered the activation temperatures from 1200 K - 1300 K to 1000 K - 1100 K to see if this would reduce the brightness in the WISE bands while leaving the Gaia light curve unchanged. Figure 19 shows that the W1 and W2 magnitudes became only slightly fainter. The main effect was to have the optical outburst occur sooner, in better agreement with observations.

Finally, we used the same model parameters but setting the flat surface density region at  $\Sigma = 4000 \text{ g cm}^{-2}$  rather than at  $2000 \text{ g cm}^{-2}$ . As expected, this results in a higher accretion rate by roughly a factor of two (Figure 10). The G magnitudes are in better agreement with observations, but now W1 and W2 are too bright.

These results show that we have been unable to significantly change the ratio of disc infrared and optical fluxes during outburst. Changes in accretion rate simply end up being reflected in the emission at both wavelength regions. This isn't particularly surprising to the extent that the disc temperature distribution during outburst is similar to that of a steady disc. However, there is a subtlety in the model calculations that enhances the infrared relative to the optical in comparison with a steady disc. As shown in Figure 20, the time-dependent models show an elevated surface temperature relative to a steady-disc power-law distribution. The reason for this is that the adopted dust opacity disappears above  $T \sim 1500 \text{ K}$ . Since the gas opacity at slightly higher temperatures is quite small, this results in pinning the temperatures near this transition. This would not matter if the accretion rate was precisely independent of radius, but it is time-dependent. This region of elevated temperature results in the WISE fluxes being about 0.5 mag brighter than would be the case for the dot-dash temperature distribution.

In summary, our results show that the behavior of Gaia 17bpi can be reasonably approximated by a temperature perturbation activating the MRI at a radius  $\sim 0.1 \text{ au}$  and  $\alpha = 0.1$ . These results are similar

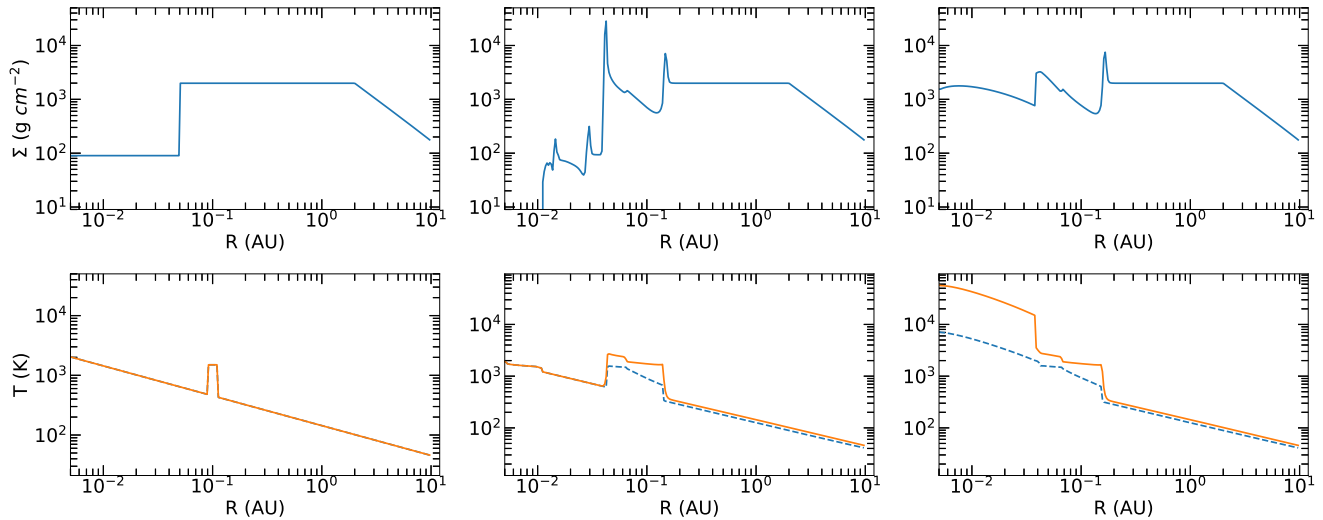


**Figure 15.** Initial conditions for a first attempt at modeling Gaia 17bpi (see text).

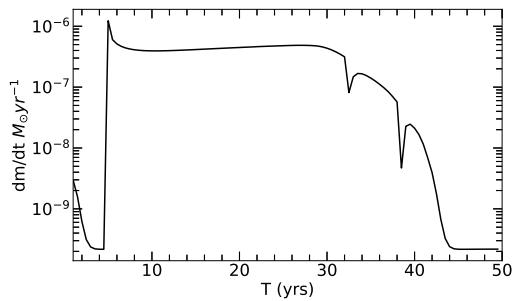


**Figure 16.** Accretion rate vs. time for model shown in Figure 15.

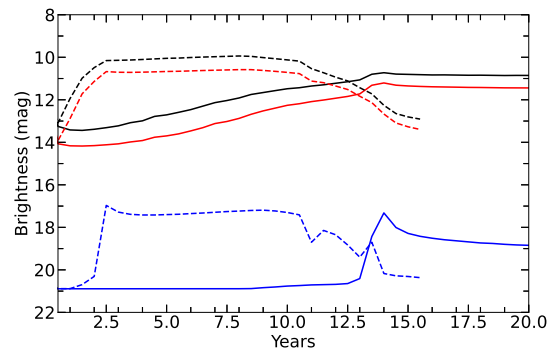


**Figure 18.** Light curves calculated for the same structural model  $\Sigma$  and  $T$  as in Figures 15 for a viscosity parameter of  $\alpha = 0.03$  (solid curves) and a reduction in the surface density by a factor of three for the  $\alpha = 0.3$  case (dashed lines). The high viscosity results in a very quick onset of the optically-visible burst, with very little lag time from the infrared, while  $\alpha = 0.03$  yields a much longer lag time than observed in Gaia 17bpi.

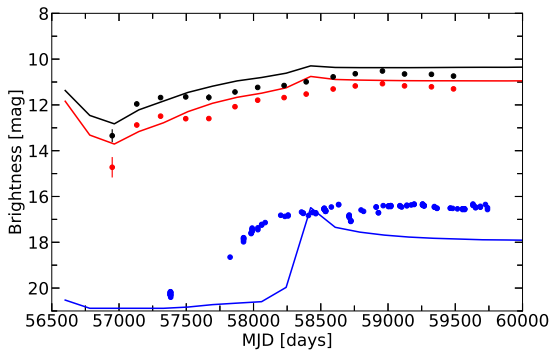


**Figure 17.** Light curves for the simulation shown in Figures 15 and 16.

to the estimate of Liu et al. (2022) of the same  $\alpha$  and a starting radius of 0.07 au based on a simple model of outburst propagation. The ratio of infrared to optical emission in our models is larger than observed if  $A_V = 3.5$ ; decreasing this by  $\sim 1$  magnitude would result in much better agreement, and might be within observational uncertainties (see, e.g. Hillenbrand et al. 2018). The discrepancy might also reflect limitations in our 1-dimensional  $\alpha$  models, which predict a sharper optical rise than observed.

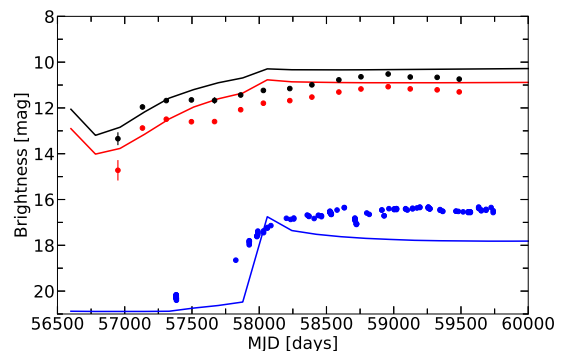


**Figure 19.** Light curve comparison with the same surface density distribution and temperature perturbation as in Figure 15, but lowering the temperature onset of the MRI to occur between 1000 K and 1100 K (see text).

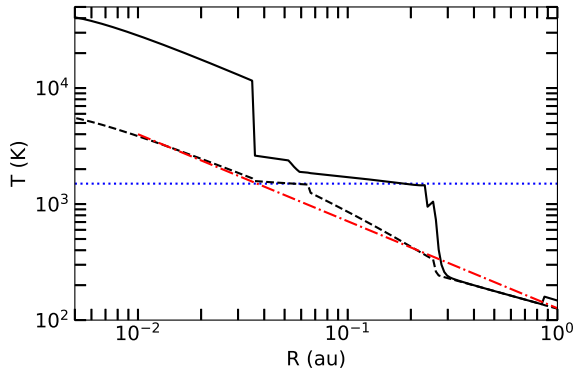


**Figure 20.** Comparison of disc temperatures for the model in Figures 7 and 9 with that of a simple steady disc  $T \propto R^{-3/4}$  at a time  $t = 20$  yr. The model exhibits an excess relative to the power-law behavior between about 0.4 and 2 au (see text).